

Propagating wave-packets and quantised currents in coherently driven polariton superfluids

M. H. Szymańska,¹ F. M. Marchetti,² and D. Sanvitto³

¹*Department of Physics, University of Warwick, Coventry, CV4 7AL, UK**

²*Departamento de Física Teórica de la Materia Condensada, Universidad Autónoma de Madrid, Madrid 28049, Spain*

³*Departamento de Física de Materiales, Universidad Autónoma de Madrid, Madrid 28049, Spain*

(Dated: May 25, 2010)

We study the properties of propagating polariton wave-packets and their connection to the stability of doubly charged vortices. Wave-packet propagation and related photoluminescence spectra exhibit a rich behaviour dependent on the excitation regime. We show that, because of the non-quadratic polariton dispersion, doubly charged vortices are stable only when initiated in wave-packets propagating at small velocities. Vortices propagating at larger velocities, or those imprinted directly into the polariton optical parametric oscillator (OPO) signal and idler are always unstable to splitting.

PACS numbers: 42.65.Yj, 47.32.C-, 71.36.+c

After almost a decade since the first reports of bosonic stimulation [1, 2], resonantly pumped polaritons have been shown to exhibit a new form of non-equilibrium superfluid behaviour [3–5]. The experimental ability to control externally the polariton currents (phase variations) with the laser pump [4] as well as to generate propagating polariton wave-packets (density and phase variations), by applying another pulsed laser probe [3], is a unique feature of driven polariton systems. Here, the interplay between phase and amplitude variations opens the possibility for novel superfluid phenomena. In addition, by using a pulsed Laguerre-Gauss beam, polaritons in the optical parametric oscillator (OPO) regime have been recently shown to display persistence of currents and metastability of quantum vortices with charge $m = 1$ and $m = 2$ [5].

In this Letter we report a comprehensive theoretical analysis of propagating polariton wave-packets, triggered by a pulsed probe, and examine the stability of vortices of charge $m = 2$ in different excitation regimes. In particular, we assess how the wave-packet shape, velocity and intensity, as well as the stability of $m = 2$ vortices, are related to the probe wavevector and to the photoluminescence (PL) spectra. The behaviour of $m = 2$ vortices has been studied recently [5], and two distinct regimes have been singled out: In the TOPO regime the initiated vortex only lasts for as long as the additional decaying gain introduced by the triggering probe. Here, $m = 2$ vortices have been shown to be remarkably stable when initiated at small group velocities and instead to split into two $m = 1$ vortices at larger velocities. In a second regime, vortices have been shown to withstand the gain and imprint into the OPO. In this case, $m = 2$ vortices always split. We provide the theoretical explanation for this intriguing phenomena.

The behaviour of $m = 2$ vortices has been the subject of intensive research in the context of ultra-cold atomic

gases. However, although stable free $m = 2$ vortices have been predicted for specific ranges of density and interaction strength [6, 7], they have not been observed experimentally [8]. Stable pinned $m = 2$ persistent currents have been recently realised [9] only by using toroidal traps.

Model The time evolution of coherently driven polaritons is described by the Gross-Pitaevskii equations for coupled cavity photon and exciton fields $\psi_{C,X}(\mathbf{r}, t)$ with pump and decay ($\hbar = 1$) [10]:

$$i\partial_t \begin{pmatrix} \psi_X \\ \psi_C \end{pmatrix} = \begin{pmatrix} 0 \\ F_p + F_{pb} \end{pmatrix} + \begin{pmatrix} \omega_X - i\kappa_X + g_X|\psi_X|^2 & \Omega_R/2 \\ \Omega_R/2 & \omega_C - i\kappa_C \end{pmatrix} \begin{pmatrix} \psi_X \\ \psi_C \end{pmatrix}. \quad (1)$$

We use here the same notation as in Ref. [11]. The cavity field is driven by a continuous-wave pump, $F_p(\mathbf{r}, t) = \mathcal{F}_{f_p, \sigma_p}(r)e^{i(\mathbf{k}_p \cdot \mathbf{r} - \omega_p t)}$ with a Gaussian or a top-hat spatial profile $\mathcal{F}_{f_p, \sigma_p}$ of strength f_p and full width at half maximum (FWHM) σ_p . $F_{pb}(\mathbf{r}, t)$ is the pulsed probe introduced later. We neglect the exciton dispersion and assume a quadratic dispersion for photons, $\omega_C = \omega_C^0 - \frac{\nabla^2}{2m_C}$. Ω_R is the Rabi splitting and the fields decay with rates $\kappa_{X,C}$. The exciton interaction strength g_X is set to one by rescaling both fields $\psi_{X,C}$ and pump strength F_p and F_{pb} by $\sqrt{\Omega_R/(2g_X)}$. Through the paper, $m_C = 2 \times 10^{-5}m_0$, the energy zero is set to $\omega_X = \omega_C^0$ (zero detuning) and $\Omega_R = 4.4\text{meV}$. We numerically solve Eq. (1) on a 2D grid using 5th-order adaptive-step Runge-Kutta algorithm.

In the absence of the probe ($F_{pb} = 0$), polaritons are continuously injected into the *pump* state and, above the pump strength threshold for OPO, f_p^{th} , undergo stimulated scattering into the *signal* and *idler* states [2] (see Fig. 1 left panels). We filter the signal, idler and pump spatial profiles $|\psi_{C,X}^{s,i,p}(\mathbf{r}, t)\rangle e^{i\phi_{C,X}^{s,i,p}(\mathbf{r}, t)}$ in a cone around their associated momenta $\mathbf{k}_{s,i,p}$. The supercur-

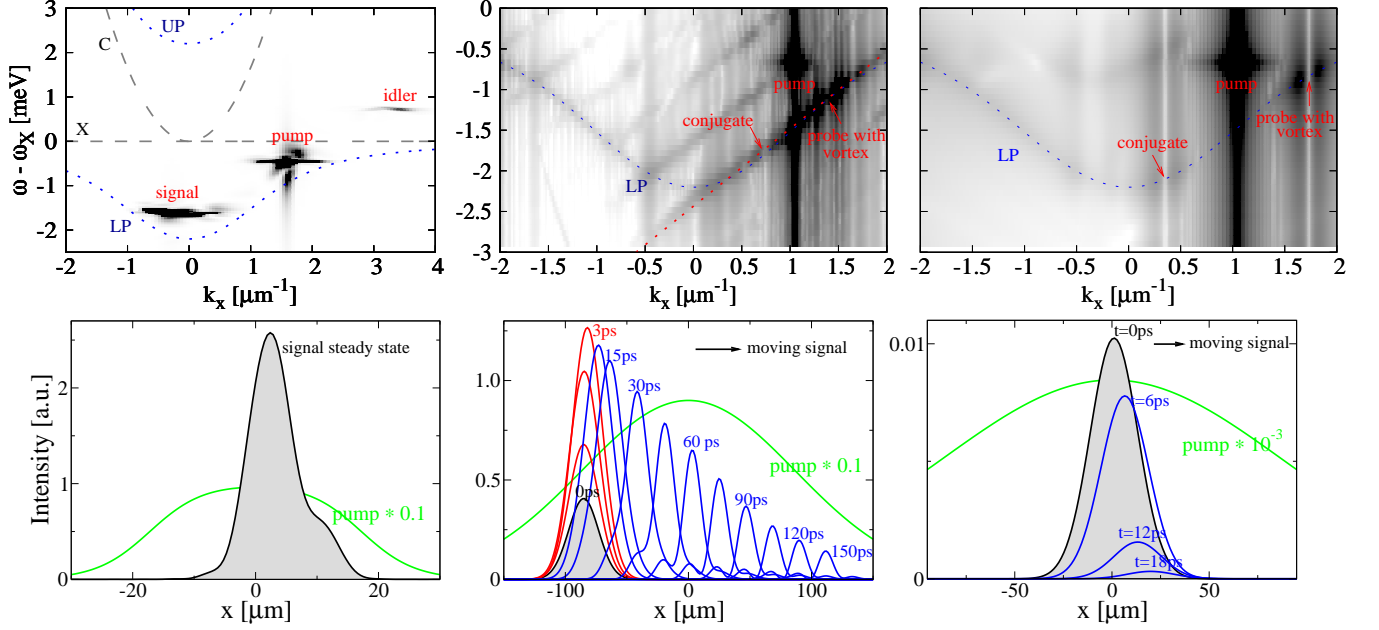


FIG. 1: (Color online) PL spectra (top) and spatial profiles of pump and filtered signal $|\psi_C^s(x, 0, t)|$ (bottom) for three regimes: (i) OPO (left panels) for a smoothen top-hat pump above threshold ($f_p = 1.12f_p^{\text{th}}$): polaritons, continuously injected at $(k_p, 0)$ and ω_p , undergo stimulated scattering into signal and idler stationary steady states ($\kappa_{X,C} = 0.2\text{meV}$). (ii) TOPO (middle panels): a short, $\sigma_t = 1\text{ps}$, Laguerre-Gauss $m = 2$ (top) and Gaussian $m = 0$ (bottom) probe (2) resonant with $(k_{pb}, 0)$ and ω_{pb} triggers propagating signal and conjugate states, which lock to the same group velocity ($\kappa_X = 0$, $\kappa_C = 0.02\text{meV}$). (iii) Similar conditions to (ii) but $\kappa_{X,C} = 0.09\text{meV}$ (right panels); now there is no amplification of the probe, both signal and conjugate decay exponentially. Lower (LP) and upper (UP) polariton (blue dashed lines), and bare cavity photon (C) and exciton (X) dispersions (gray dashed lines) are shown for reference.

rent, $\nabla\phi_{C,X}^{s,i,p}$, is a superposition of the dominant uniform flow $\mathbf{k}_{s,i,p}$ and more complex currents (caused by the system being finite size), which move particles from gain to loss dominated regions. In addition one can characterise the density variations defining the *group velocity* $\mathbf{v}_g^{s,i,p} = d\mathbf{r}_m^{s,i,p}/dt$, where $\mathbf{r}_m^{s,i,p}$ is the maximum of the signal (idler and pump) spatial profile. The OPO is a steady state regime, where $|\psi_{C,X}^{s,i,p}(\mathbf{r}, t)|$ are time independent. This is also recognisable in the typical flat dispersion of signal, idler and pump PL spectra (see left panel of Fig. 1) — the signal (idler, pump) group velocity being the derivative of the dispersion at \mathbf{k}_s ($\mathbf{k}_{i,p}$).

Propagating wave-packets and TOPO regime In order to create propagating wave-packets (finite group velocity), one needs to add a pulsed probe with finite momentum \mathbf{k}_{pb} , spatially small with respect to the pump spot size [3]. Since we are interested in the stability of triggered vortices of charge $m = 2$, and its connection to the character of the propagating wave-packet, we consider here a Laguerre-Gauss pulsed probe [5, 11, 12],

$$F_{pb}(\mathbf{r}, t) = f_{pb} |\mathbf{r} - \mathbf{r}_{pb}|^{|m|} e^{-|\mathbf{r} - \mathbf{r}_{pb}|^2 / (2\sigma_{pb}^2)} e^{im\varphi} \times e^{i(\mathbf{k}_{pb} \cdot \mathbf{r} - \omega_{pb}t)} e^{-(t-t_{pb})^2 / (2\sigma_t^2)}, \quad (2)$$

where the phase φ winds from 0 to 2π around the vortex core \mathbf{r}_{pb} . Above threshold for OPO, $f_p > f_p^{\text{th}}$, one can

identify two distinct regimes depending on the system parameters [5]: In one case, the triggered vortex propagates as extra population (gain) on top of the OPO stationary signal and idler states [3] — TOPO regime. Here, the vortex lasts only for as long as the additional decaying gain. A similar TOPO regime can be found also below the OPO threshold, and for simplicity we show this case in Fig. 1 (middle panel). Alternatively, vortices persist the gain and get imprinted into the OPO signal and idler — metastable vortex regime [11].

In the TOPO regime, the polaritons generated by the probe scatter parametrically with the ones of the pump, generating a traveling signal (here meant as extra population on top of either the OPO signal or idler, or full signal if below the OPO threshold) with momentum $\mathbf{k}_s = \mathbf{k}_{pb}$ (which can be either $\mathbf{k}_{pb} > \mathbf{k}_p$ or $\mathbf{k}_{pb} < \mathbf{k}_p$) and its *conjugate* at $\mathbf{k}_c = 2\mathbf{k}_p - \mathbf{k}_{pb}$. In the case of the middle panels of Fig. 1 the signal and the conjugate get initially strongly amplified by the parametric scattering from the pump state, then decay slowly (we refer to this as a proper TOPO regime) and, at later times, eventually the decay becomes exponential. This regime reproduces the one observed in experiments (see Fig. 3 of Ref. [14]), where the intensity maximum is reached quickly, within 4ps after the maximum of the pulsed probe, and is immediately followed by a slow decay. Instead, for the case of the

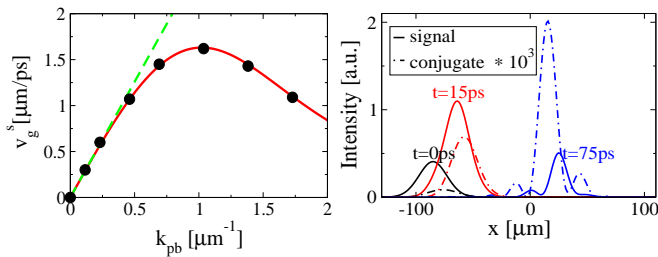


FIG. 2: (Color online) Left panel: Group velocity, v_g^s of the propagating signal wave-packet as a function of the probe momentum k_{pb} . The black dots are determined from simulations, whereas the solid line (red) is the derivative of the LP dispersion evaluated at k_{pb} , $v_{k_{pb}}^{LP}$. The green dashed line indicates where the LP dispersion deviates from the quadratic behaviour. Right panel: Signal (solid lines) and conjugate (dashed lines) states for $k_{pb} = 1.4\mu\text{m}^{-1}$ at different times after the arrival of the probe.

right panels of Fig. 1, parametric scattering is too weak to induce any significant amplification, and we observe exponential decay of signal and conjugate populations immediately after the probe switches off.

By analysing the change in time of the spatial profile of the TOPO signal $|\psi_{C,X}^s(\mathbf{r}, t)|$, we find that its group velocity v_g^s is simply given by the derivative of the lower polariton (LP) dispersion evaluated at \mathbf{k}_{pb} , i.e. for zero detuning and low densities by $v_{k_{pb}}^{LP} \equiv k_{pb}/(2m_C) - k^3/(2m_C\sqrt{k^4 + 4m_C^2\Omega_R^2})$ (see Fig. 2). We have confirmed this for both TOPO regimes.

In order to understand this result it is instructive to analyse the PL spectra. In the regime with weak parametric scattering (right panel of Fig. 1), aside the strong emission from the pump state, the dispersion is simply that of the LP, and thus the signal propagates with a group velocity given by $v_{k_{pb}}^{LP}$. However, in the proper TOPO regime (middle panel of Fig. 1) the spectrum becomes linear. This can be explained by the fact that in order to have efficient parametric scattering processes, signal and conjugate require a large spatial overlap and so their group velocities need to lock to the same value, therefore the dispersion becomes linear — a similar result has been found in 1D simulations, as well as in experiments [3]. Here, we determine that the TOPO linear dispersion is tangential to the LP branch at k_{pb} , thus its slope is given in this case also by $v_{k_{pb}}^{LP}$.

The linearisation of the TOPO dispersion, with the slope defined by the probe momentum k_{pb} , also explains our observation that the TOPO amplification is stronger when signal ($\mathbf{k}_s = \mathbf{k}_{pb}$) and conjugate (\mathbf{k}_c) wavevectors (connected via parametric constraint $2\mathbf{k}_p = \mathbf{k}_s + \mathbf{k}_c$) have nearby values. This implies that the LP tangential line at \mathbf{k}_{pb} lies close to the LP dispersion also at \mathbf{k}_c , therefore leading to efficient stimulation. It is interesting to note, that by changing \mathbf{k}_p and \mathbf{k}_{pb} it is possible to engineer

wave-packets with a broad range of values of group velocities and supercurrents — e.g., for $\mathbf{k}_{pb} = 2\mathbf{k}_p$, one has a conjugate state at $\mathbf{k}_c = 0$ (i.e., no net current) with a large group velocity, $v_g^c = v_{2k_p}^{LP}$.

From the PL spectrum we can deduce the nature of the wave-packet propagation. For linear dispersion one expects a soliton-like behaviour, with signal and conjugate propagating and not changing neither shape nor intensity. For quadratic dispersion, propagation is analogous to the ballistic time-of-flight expansion of ultracold atomic gases [13], i.e. for a Gaussian wave-packet, the $\text{FWHM} = (\sigma_{pb}^2 + (\frac{t}{2m_C\sigma_{pb}})^2)^{1/2}$ grows in time, but the shape is preserved. The total density decays exponentially with rate given by $\frac{\kappa_C + \kappa_X}{2}$ at zero detuning, and the maximum of the wave-packet moves with a constant velocity $v_{k_{pb}}^{LP}$ (equal to $\frac{k_{pb}}{2m_C}$ in the quadratic LP regime). Due to the dynamical nature of the TOPO state, the system evolves between different regimes. In particular, only in the strong amplification regime the spectrum is linear, while it evolves back to LP at longer times. In addition, when the LP dispersion deviates from quadratic, propagation becomes complex: the wave-packet gets distorted and one observes beatings in the spatial profiles.

Propagation of signal and conjugate are shown in the right panel of Fig. 2. We observe a mechanism analogous to the one found in four-wave-mixing experiments [15, 16]: when the probe arrives the conjugate propagates faster than the signal, before getting locked to it with a small spatial shift of their maximum intensities. At later times, when the density drops and the parametric process becomes inefficient, the two wave-packets start unlocking — the conjugate slows down with respect to the signal if $k_c < k_s$ as in Fig. 2, or moves faster when $k_c > k_s$.

Stability of $m = 2$ TOPO vortices In the TOPO regime, we observe $m = 2$ vortices to be stable within their lifetime when triggered at small momenta k_{pb} (Fig. 3a,c), while TOPO vortices always split into two $m = 1$ vortices for large k_{pb} (Fig. 3b,d), in agreement with the recent experimental observations [5]. Our numerical analysis shows that the crossover from non-splitting to splitting happens for values of the probe momentum where the LP dispersion deviates from quadratic (see Fig. 2). The two regimes are shown in Fig. 3: For $k_{pb} = 0.2\mu\text{m}^{-1}$, at short times, the signal carrying the vortex propagates without changing shape and with little change in intensity, consistent with the corresponding PL spectrum having a linear dispersion. However, at longer times the density drops more than two orders of magnitude, the dispersion becomes quadratic and therefore the wave-packet expands (panel c). A uniform expansion of the wave-packet leads to the increase of the vortex core but does not cause the vortex to split. In contrast, for $k_{pb} = 1.4\mu\text{m}^{-1}$, where the LP dispersion is not quadratic, the splitting of the $m = 2$ vortex state into two $m = 1$ vortices happens shortly after the arrival of the probe (panel d). This behaviour can be explained

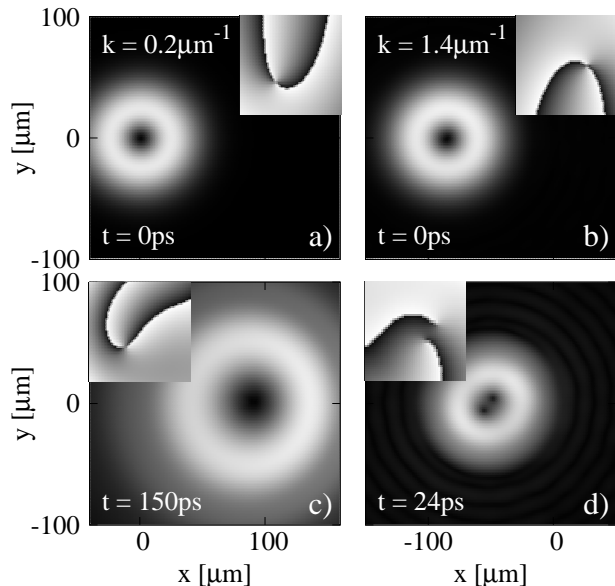


FIG. 3: Profiles of TOPO signal intensity $|\psi_C^s(\mathbf{r}, t)|$ and phase $\phi_C^s(\mathbf{r}, t)$ (inset) after the arrival (at $t = 0$) of an $m = 2$ vortex pulsed probe (2) with $\sigma_{pb} \simeq 87 \mu\text{m}$. The conditions are the same as the middle panels of Fig. 1, but with $k_{pb} = 0.2 \mu\text{m}^{-1}$ (a,c) and $k_{pb} = 1.4 \mu\text{m}^{-1}$ (b,d). While in the case (a,c) the $m = 2$ vortex does not split within its lifetime, in (b,d) the vortex splits soon after the probe arrives. The intensity scale in (c) is 200 times smaller than in (a) – signal expands as the density drops two orders of magnitude (see text).

as follows: the dispersion of the time-dependent TOPO evolves from LP (before the probe arrival) to linear (at early times after the probe arrival), and back to the LP dispersion at later times. Wave-packets propagating with non-quadratic dispersion do not keep their shapes. Indeed, we see the distortion to be very pronounced at later times of the evolution. This distortion during the propagation leads to the mechanical splitting of $m = 2$ vortex, analogous to the structural instability discussed in [17]. Also, as discussed in [5], for small k_{pb} , within the quadratic part of the dispersion, the group velocity of the propagating vortex and the velocity associated with the net supercurrent (given by k_{pb}) are equal. However, this is not the case for larger k_{pb} , beyond the quadratic part, and so the propagating vortex feels rather strong net current in its frame, which may provide additional explanation for splitting.

$m = 2$ vortices imprinted into the OPO As in Ref. [5], we find that doubly charged ($m = 2$) vortices which get imprinted into the OPO signal are never stable, and split into two $m = 1$ vortices almost immediately, even before the probe reaches its maximum intensity, as shown in Fig. 4. There are several causes of the splitting: Before the probe arrives, the OPO dispersion is flat around the signal, idler, and pump. However, the triggering probe

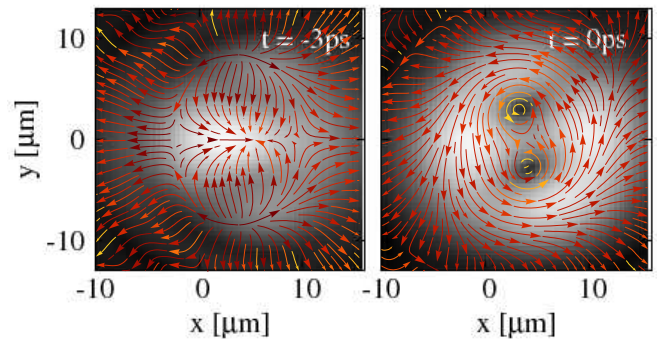


FIG. 4: (Color online) Filtered signal profile and currents above OPO threshold $f_p = 1.12 f_p^{(\text{th})}$ for a top-hat pump with FWHM $\sigma_p = 35 \mu\text{m}$ at $t = -3 \text{ps}$ (left panel) before the arrival of an $m = 2$ probe at $t = 0 \text{ps}$ (right). The double quantised vortex splits into two $m = 1$ vortices even before the probe reaches its maximum intensity.

favours the signal and conjugate to lock and propagate with the same velocity $v_{k_{pb}}^{LP}$, which corresponds to a linear dispersion. Further, once the vortex gets imprinted into the stationary OPO signal and idler, the dispersion changes back to be flat. The evolution of the dispersion between linear and flat leads to a complicated dynamics of both signal and idler (the *transient period* described in [11]), causing the structural instability and splitting of the vortex during the transient time. Another reason for the structural instability during the vortex imprinting into the OPO signal and idler are the non-uniform currents (shown in Fig. 4) caused by the interplay between spatial inhomogeneity, pump and decay, which the OPO vortex experiences in its reference frame.

To conclude, we have determined group velocity and supercurrents of propagating polariton wave-packets triggered by a short pulsed laser probe, and established the conditions under which triggered $m = 2$ vortices are stable and when they split into two vortices of $m = 1$. Both phenomena are related to the form of the PL spectrum as well as the wave-vector of the triggering probe. The ability to control the topological charge and number of vortices, simply by changing the wave-vector of the external probe, holds potential for operations in quantum information. In addition, we have shown that, by varying the pump and probe wavevectors, it is possible to engineer polariton wave-packets with any relation between group and supercurrents velocities — a property which can be useful for storage applications.

We are grateful to E. Cancellieri, J. Keeling, C. Tejedor and L. Viña for stimulating discussions. F.M.M. and D.S. acknowledge financial support from the programs Ramón y Cajal and INTELBIOMAT (ESF). We thank TCM group (Cavendish Laboratory, Cambridge) for the use of computer resources.

-
- * also at London Centre for Nanotechnology, UK
- [1] P. G. Savvidis, et al., Phys. Rev. Lett. **84**, 1547 (2000).
 - [2] R. M. Stevenson, et al., Phys. Rev. Lett. **85**, 3680 (2000).
 - [3] A. Amo, et al., Nature **457**, 291 (2009).
 - [4] A. Amo, et al., Nat. Phys. **5**, 805 (2009).
 - [5] D. Sanvitto, et al. Nat. Phys. in press (2010), arXiv:0907.2371.
 - [6] H. Pu, C. K. Law, J. H. Eberly, and N. P. Bigelow, Phys. Rev. A **59**, 1533 (1999).
 - [7] M. Möttönen, et al., Phys. Rev. A **68**, 023611 (2003).
 - [8] Y. Shin, et al., Phys. Rev. Lett. **93**, 160406 (2004).
 - [9] C. Ryu, et al., Phys. Rev. Lett. **99**, 260401 (2007).
 - [10] D. M. Whittaker, phys. stat. sol. (c) **2**, 733 (2005).
 - [11] F. M. Marchetti, M. H. Szymańska, C. Tejedor, and D. M. Whittaker (2010), arXiv:1003.5111.
 - [12] D. Whittaker, Superlatt. and Microstruct. **41**, 297 (2007).
 - [13] L. P. Pitaevskii and S. Stringari, *Bose-Einstein Condensation* (Clarendon Press, Oxford, 2003).
 - [14] G. Tosi, et al., Journal of Physics: Conference Series **210**, 012023 (2010).
 - [15] V. Boyer, C. F. McCormick, E. Arimondo, and P. D. Lett, Phys. Rev. Lett. **99**, 143601 (2007).
 - [16] A. M. Marino, et al., Phys. Rev. Lett. **101**, 093602 (2008).
 - [17] J. J. García-Ripoll, G. Molina-Terriza, V. M. Pérez-García, and L. Torner, Phys. Rev. Lett. **87**, 140403 (2001).